http://eprints.gla.ac.uk/225053/

Deposited on 11 December 2020

Bandwidth enhancement in an InGaN/GaN three-section superluminescent diode for optical coherence tomography

Graham R. Goldberg[1], Dae-Hyun Kim[1 a)], Richard J. E. Taylor[1], David T. D. Childs[1], Pavlo Ivanov[1], Nobuhiko Ozaki[2], Kenneth L. Kennedy[3], Kristian M. Groom[3], Yukihiro Harada[4] and Richard A. Hogg[1]

[1] *School of Engineering, University of Glasgow, Glasgow G12 8LT, United Kingdom*

[2] *Faculty of Systems Engineering, Wakayama University, 930 Sakaedani, Wakayama 640-8510, Japan*

[3] *Department of Electronic and Electrical Engineering, University of Sheffield, Sheffield 3 Solly Street S3 7HQ, UK*

[4] *Department of Electrical and Electronic Engineering, Graduate School of Engineering, Kobe University, 1-1 Rokkodai, Nada, Kobe 657-8501, Japan*

Abstract

In this paper, the optoelectronic properties of InGaN-based blue (430 nm) superluminescent light-emitting diodes with a multi-section, three contact designs are reported. The bias conditions of the rear absorber section and gain sections are explored in terms of enhancing and maximizing spectral bandwidth. We demonstrate that broader emission can be obtained with a short circuit, rather than an open circuit absorber section, and with two active regions under different current densities as opposed to a single active contact. Under optimal drive conditions, a -3dB linewidth of 20 nm is obtained at 430 nm. Analysis of the device emission spectrum indicates that ~3.4 μm axial resolution may be obtained in an optical coherence tomography system.

For non-invasive biomedical imaging applications including ophthalmology, cardiology, and dermatology, optical coherence tomography (OCT) with high-resolution, a wide imaging range, and short acquisition time is indispensable [1–3]. OCT is dependent on temporal coherence interferometry, and the axial resolution(l_c) of OCT system is governed by the bandwidth ($\Delta\lambda$) and central wavelength (λ_0) of the light source. For an ideal broadband source with a Gaussian spectrum, it can be shown that [4]

$$l_c = \frac{2\ln(2)}{\pi} \frac{\lambda_0^2}{\Delta\lambda} \qquad (1)$$

Broader bandwidth sources improve the axial resolution in OCT and enable the system to distinguish finer features. Moderate power (often limited by eye safety) is also required from these devices to enable deeper imaging depths due to the scattering nature of biological tissue.

To date, in biomedical applications, central wavelengths in the near-infrared (NIR) range have been preferred because of lower scattering in skin tissue and the availability of light sources; with tuneable lasers and superluminescent light emitting diodes (SLEDs) the most common commercial sources for OCT.

Recently, the increased demand for improved axial resolution has led to the extension of wavelengths used for OCT. For example, it has been reported that the ultraviolet and visible-wavelength bands can be used for in-situ OCT imaging of the dermal layer [5]. However, the light sources disclosed require complex supplementary systems [6], yet highlight the benefit of reducing the magnitude of the numerator in Eq. (1) as compared to that for NIR sources. As such, GaN-based SLEDs are increasingly attractive for OCT applications owing to their short wavelength and broad emission spectra. This will result in not only enhanced axial and lateral resolutions but also an increased signal-to-noise ratio. Sub-cellular axial resolution is also possible if broader bandwidth shorter wavelength SLEDs can be realized [7].

In this letter, we report on the three-section InGaN-based SLED devices to increase the spectral bandwidth. We show that by careful control of the current injection into forward bias sections, and the choice of a short circuit (S/C) absorber, as opposed to open circuit (O/C), the emission bandwidth can be increased from 13 nm to 20 nm. The broadest emission spectrum we obtained indicates OCT imaging resolutions of 3.4 μm may be obtained,

---

a)Electronic mail: Daehyun.Kim@glasgow.ac.uk

paving the way for low-cost, robust sub-cellular resolution OCT systems.

A metalorganic chemical vapor deposition (MOCVD) system was used to grow blue (430 nm) InGaN/GaN-based SLED structures on freestanding c-plane GaN substrate with a dislocation density in the $1 - 5 \times 10^6$ cm^{-2} range. The epilayer stack consists of 1 µm Si-doped n-GaN ($n_d = 3 \times 10^{18}$ cm^{-3}), 1 µm cladding layer of Si-doped Al$_{0.07}$Ga$_{0.93}$N ($n_d = 1 \times 10^{18}$ cm^{-3}), an active region of two 4.5 nm In$_{0.12}$Ga$_{0.88}$N/GaN quantum wells (QW), separated by 11.5 nm GaN barrier, 20 nm electron blocking layer of Mg-doped Al$_{0.2}$Ga$_{0.8}$N ($n_a = 1 \times 10^{17}$ cm^{-3}), 110 nm Mg-doped GaN, 0.5 µm cladding layer of Mg-doped Al$_{0.06}$Ga$_{0.94}$N ($n_d = 1 \times 10^{17}$ cm^{-3}) and 50 nm Mg-doped p-GaN.

Devices were fabricated using standard photo-lithography, and the ridge waveguides were etched below the active region using a plasma-enhanced chemical vapor deposition (PECVD) silicon dioxide mask and inductively-coupled plasma reactive-ion etch (ICP-RIE) process. 300 nm SiO$_2$ was deposited as an insulating layer by PECVD, Ni/Au and Ti/Al/Ti/Au ohmic contacts were deposited on the p-GaN and n-GaN layers, respectively. Device facets are as cleaved, with a normal front facet, and an angled rear facet at ~30° to the normal.

Schematic diagrams of the ~2600 µm long three-section InGaN SLEDs are shown in Fig. 1(a) and (b), where the ridge width (W$_R$) is 5 µm, and gain sections (L$_a$, L$_b$) are 870 µm. The rear absorber section (L$_{Abs}$) is 850 µm. The two gain sections, L$_a$ and L$_b$, may be biased at different current densities J$_a$ and J$_b$, which allows control of the spectral shape, output power and the amplified spontaneous emission (ASE).

Cavity suppression through the use of passive absorbers in SLEDs have been widely studied [8–10]. However, unlike (001) GaAs and InP-based devices, c-plane (0001) GaN-based devices exhibit spontaneous and piezoelectric polarization effects at internal interfaces causing strong electric fields in QWs, even at zero bias [11]. Additionally, for p-i-n structures, a forward bias increases the electric field in QWs due to field-sharing [12–14]. The calculated band diagrams of two InGaN/GaN-based QWs under zero and forward bias are plotted in Fig. 2.

Energy levels were calculated using the single-band Schrodinger equation for the conduction band, and by 6-band k.p theory for the valence band. Fundamental transition energies of the InGaN-based QWs are 2.97 (n side: "QW$_1$") and 2.94 eV (p side: "QW$_2$"), respectively, at zero bias. These transition energies blue-shift by ~0.01 eV at a forward bias of 3.4 V due to the reduction in electric field.

Typical designs of InGaN-based SLEDs are based on laser diodes with cavity suppression. For example, design of the ridge waveguide [15–18], oblique or wet etched facet [19–21], and/or absorber sections in the resonator [8]. These methods increase mirror or waveguide loss for efficient cavity suppression. However, previous designs have a limited emission bandwidth (~10 nm). To realize improved axial resolution through bandwidth enhancement of the InGaN-based blue SLEDs, an angled back facet (~30°) and normal front facet are utilised to obtain a simple far-field pattern. To increase cavity suppression, the rear section is operated as an absorber. The absorber section can be operated in O/C, S/C or reverse-biased modes.

Only limited work has been performed on the use of absorber sections in InGaN-based SLEDs. Kwong et al. investigated the electrical and optical properties of O/C absorber sections in GaAs SLEDs, demonstrating that GaAs-based SLEDs with O/C absorber sections had increased lasing thresholds. However, at high current injection, the O/C absorber became optically pumped, and lasing was observed due to burn through [9].

We previously demonstrated that operating the absorber section of a dual-section SLED in S/C resulted in broader emission than operating the absorber in O/C [22]. This was attributed to the recycling of backward-propagating light in the SLED, which is at a different wavelength in the case of S/C absorbers due to screening effects of photo-carriers in the QW structures [23]. At high current injection, the absorbed backward propagating light induces a photo-voltage in the O/C absorber section, blue-shifting the emission to be close to that of the forward biased p-n junction [24]. This means the spontaneous emission and recycled light have similar wavelengths which overlap with the gain spectra and reduce the spectral bandwidth. However, in case of an S/C absorber, the photo-voltage is not generated. Consequently, the S/C absorber section and active region have different electric fields, and absorption and emission energies. Therefore, the bias condition on the absorber section plays an important role in realizing broad spectral bandwidth SLEDs due to the re-emitted light from the absorber section back into the active region.

Fig. 3 plots the output power as a function of current density for the three-section SLED with the absorber section O/C and S/C. Here the two forward bias contacts (A and B) are operated with the same current density. This operating condition is similar to the dual-section SLEDs. For both devices at lower current densities almost identical powers are measured, whilst at higher current densities, operation with an O/C absorber shows a higher output power.

The emission bandwidth as a function of output power is plotted in Fig. 4 (Spectra shown in supplementary material S1). With the absorber S/C a consistently higher spectral bandwidth is observed, in line with our prediction concerning the overlap of the recycled light with the gain and SE spectrum. This ~1 nm difference is in good agreement with the 0.01 eV difference in transition energies between open circuit and forward bias conditions shown in Fig 2. The observed reduction in spectral bandwidth with increasing power is strong evidence of gain within the system. One may expect a reduction in

2

spectral linewidth as the absorber is bleached (burn through) and the device becomes more like a dual pass device. However, we note that in the limit of zero output power the linewidths should be identical, yet a constant difference in bandwidth (and similar modulation of the spectra due to gain) is observed at the lowest current density.

In contrast, operating the front two contacts with different current densities results in different optical properties. Here sections A and B are independently pumped, and the emission spectra under various conditions are shown in supplementary material S3. The powers and bandwidth are plotted in Fig. 5, where the effect of sharing drive current between the gain sections, and increasing current to section A of the contact is explored for O/C and S/C absorber operation, respectively. An enhancement in bandwidth is observed by using higher current densities in section A of the device at the expense of emission power.

The emission spectra of the three-section SLEDs under bias conditions that give maximum bandwidth (~3 kAcm^{-2} and ~1 kAcm^{-2} current injection on the 'A' and 'B' sections, respectively) for O/C and S/C absorber operation are shown in Fig. 6. Modulation to the top of the electroluminescence peak is strong evidence for gain within the device [9]. At drive current densities of 0.95 kAcm^{-2}, strong modulation of the peak is also observed (inset of the supplementary material S3), suggesting that the device is in gain at both current densities.

It is noteworthy that the three-section SLEDs with S/C absorber section show broader emission spectra than the SLEDs with O/C absorber section. This is due to the reduced overlap of the gain spectra and the recycled light from S/C absorber section. We note that a ~4 nm enhancement to spectral bandwidth is observed for the gain section biases in Fig. 6 in biasing the absorber in S/C as opposed to O/C. This is attributed to the sequential convolution of the emission spectrum of the recycled absorber light with the gain spectra of sections A and B, its superposition with the ASE generated in section A and amplified in section B, along with the ASE generated in section B. Additionally, irrespective of the different absorber operation, broadening of the emission bandwidth to shorter wavelengths is observed. This can be attributed to the combined effect of band filling and the quenching of photon absorption. The three-section SLEDs with different current density on the front two gain sections exhibited enhanced bandwidth properties compared with the SLEDs operated under the same current density on the front two gain sections as shown in Fig. 5.

A maximum bandwidth of 20 nm was obtained with a power of 140 μW in-line with maximum permitted exposure limits [25]. This demonstrates that the optical properties of the three-section SLEDs can be optimized by the independent control of each gain section. However, the output power is limited due to the poor overlap of emission and gain spectra of the individual elements. This trade-off of power and spectral bandwidth is well known in SLEDs due to the convolution of gain and spontaneous emission spectra [26].

Under optimal operating conditions, the three-section SLED (Fig. 6, S/C) was evaluated as an OCT light source. As the spectrum is not a perfect Gaussian profile, the axial resolution cannot be determined directly from Eq. (1). To estimate the axial resolution in an OCT system, the coherence length impacts upon the self-coherence function, which is given by the inverse Fourier transform (IFT) of the power spectral density, and can be regarded as the point-spread function of the imaging system [27]. The IFT spectrum obtained from the emission spectrum is shown in Fig. 7. This function represents the detected signal from a single reflection plane within a specimen. The axial resolution can be determined by measuring the full-width-half-maximum of the IFT spectrum. The estimated axial resolution is ~3.4 μm. We highlight that there are no significant side lobes, reducing the prospect of ghost images.

The opto-electronic properties of multi-section InGaN-based blue SLEDs have been reported. By comparison to dual-section SLEDs, three-section SLEDs with different drive conditions in their two active sections provide higher spectral bandwidths at the expense of optical power. The bias condition of the absorber section was highlighted as an additional route to enhance spectral bandwidth. Under optimal drive conditions, a 20 nm wide bandwidth with 0.14 mW of power was obtained and the IFT of the emission spectrum indicates that ~3.4 μm axial resolution may be obtained in an OCT system. The short wavelength and broad emission bandwidth of the device makes these components suitable for sub-cellular resolution of OCT system.

See supplementary material for the optical and electrical characteristics of the studied three-section InGaN-based SLEDs.

DATA AVAILABILITY

The data that supports the findings of this study are available within the article [and its supplementary material].

REFERENCE

[1] W. Drexler and J.G. Fujimoto, editors , *Optical Coherence Tomography* (Springer Berlin Heidelberg, Berlin, Heidelberg, 2008).

[2] T.E. de Carlo, A. Romano, N.K. Waheed, and J.S. Duker, Int. J. Retin. Vitr. **1**, 5 (2015).

[3] Q. Zhang, C.S. Lee, J. Chao, C.-L. Chen, T. Zhang, U. Sharma, A. Zhang, J. Liu, K. Rezaei, K.L. Pepple, R. Munsen, J. Kinyoun, M. Johnstone, R.N. Van Gelder, and R.K. Wang, Sci. Rep. **6**, 22017 (2016).

[4] *Optical Coherence Tomography* (Elsevier, 2006).

[5] H. Hirayama and S. Nakamura, J. Biomed. Opt. **20**, 076014 (2015).

[6] S. Maliszewska and M. Wojtkowski, Photonics Lett. Pol. **3**, (2011).

[7] V.R. Shidlovski, in *Opt. Coherence Tomogr.* (Springer International Publishing, Cham, 2015), pp. 505–526.

[8] A. Kafar, S. Stańczyk, S. Grzanka, R. Czernecki, M. Leszczyński, T. Suski, and P. Perlin, J. Appl. Phys. **111**, 083106 (2012).

[9] N.S.K. Kwong, K.Y. Lau, and N. Bar-Chaim, IEEE J. Quantum Electron. **25**, 696 (1989).

[10] A. Kafar, S. Stańczyk, P. Wišniewski, T. Oto, I. Makarowa, G. Targowski, T. Suski, and P. Perlin, Phys. Status Solidi Appl. Mater. Sci. **212**, 997 (2015).

[11] T. Takeuchi, S. Sota, M. Katsuragawa, M. Komori, H. Takeuchi, H. Amano, and I. Akasaki, Jpn. J. Appl. Phys. (1997).

[12] A.S. Pabla, J. Woodhead, E.A. Khoo, R. Grey, J.P.R. David, and G.J. Rees, Appl. Phys. Lett. **68**, 1595 (1996).

[13] R.A. Hogg, T.A. Fisher, A.R.K. Willcox, D.M. Whittaker, M.S. Skolnick, D.J. Mowbray, J.P.R. David, A.S. Pabla, G.J. Rees, R. Grey, J. Woodhead, J.L. Sanchez-Rojas, G. Hill, M.A. Pate, and P.N. Robson, Phys. Rev. B **48**, 8491 (1993).

[14] T. Takeuchi, C. Wetzel, S. Yamaguchi, H. Sakai, H. Amano, I. Akasaki, Y. Kaneko, S. Nakagawa, Y. Yamaoka, and N. Yamada, Appl. Phys. Lett. **73**, 1691 (1998).

[15] E. Feltin, A. Castiglia, G. Cosendey, L. Sulmoni, J.-F. Carlin, N. Grandjean, M. Rossetti, J. Dorsaz, V. Laino, M. Duelk, and C. Velez, Appl. Phys. Lett. **95**, 081107 (2009).

[16] F. Kopp, T. Lermer, C. Eichler, and U. Strauss, Appl. Phys. Express **5**, 082105 (2012).

[17] K. Anna, S. Szymon, T. Grzegorz, O. Takao, M. Irina, W. Przemek, S. Tadek, and P. Piotr, Appl. Phys. Express **6**, 92102 (2013).

[18] J. Liu, J. Wang, X. Sun, Q. Sun, M. Feng, R. Zhou, Y. Zhou, H. Gao, T. Liu, Z. Huang, and H. Yang, ACS Photonics (2019).

[19] C. Zeng, S. Zhang, J. Liu, D. Li, D. Jiang, M. Feng, Z. Li, K. Zhou, F. Wang, H. Wang, H. Wang, and H. Yang, Chinese Sci. Bull. **59**, 1903 (2014).

[20] M.T. Hardy, K.M. Kelchner, Y.-D. Lin, P.S. Hsu, K. Fujito, H. Ohta, J.S. Speck, S. Nakamura, and S.P. DenBaars, Appl. Phys. Express **2**, 121004 (2009).

[21] C. Shen, J.A. Holguin-Lerma, A.A. Alatawi, P. Zou, N. Chi, T.K. Ng, and B.S. Ooi, IEEE J. Sel. Top. Quantum Electron. (2019).

[22] G.R. Goldberg, A. Boldin, S.M.L. Andersson, P. Ivanov, N. Ozaki, R.J.E. Taylor, D.T.D. Childs, K.M. Groom, K.L. Kennedy, and R.A. Hogg, IEEE J. Sel. Top. Quantum Electron. **23**, 1 (2017).

[23] T.E. Sale, J. Woodhead, G.J. Rees, R. Grey, J.P.R. David, A.S. Pabla, P.J. Rodriguez-Gíronés, P.N. Robson, R.A. Hogg, and M.S. Skolnick, J. Appl. Phys. **76**, 5447 (1994).

[24] J.P.R. David, T.E. Sale, A.S. Pabla, P.J. Rodríguez-Gironés, J. Woodhead, R. Grey, G.J. Rees, P.N. Robson, M.S. Skolnick, and R.A. Hogg, Appl. Phys. Lett. **68**, 820 (1996).

[25] X. Shu, L. Beckmann, Y. Wang, I. Rubinoff, K. Lucy, H. Ishikawa, G. Wollstein, A.A. Fawzi, J.S. Schuman, R. V. Kuranov, and H.F. Zhang, Quant. Imaging Med. Surg. (2019).

[26] Y.C. Xin, A. Martinez, T. Saiz, A.J. Moscho, Y. Li, T.A. Nilsen, A.L. Gray, and L.F. Lester, IEEE Photonics Technol. Lett. **19**, 501 (2007).

[27] M. Rossetti, P. Bardella, and I. Montrosset, Opt. Quantum Electron. **40**, 1129 (2008).
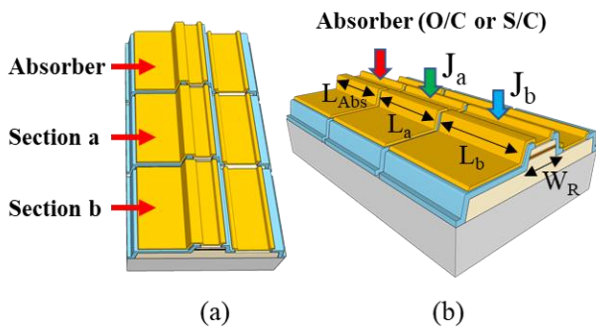
FIG. 1. Schematic diagrams of InGaN-based three-section SLEDs (a) and device structure (b).
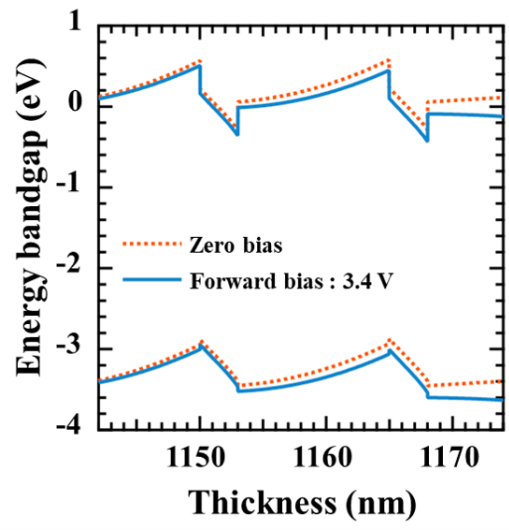
FIG. 2. Schematic band diagrams of InGaN/GaN-based QWs under zero and forward bias at 300K.
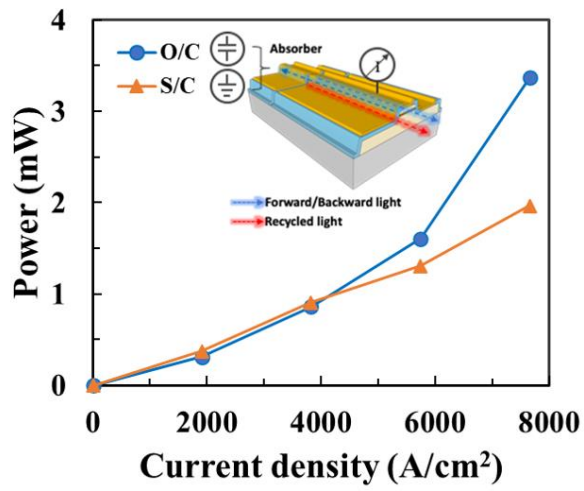
FIG. 3. Output power as a function of current density (L-J) for the three-section SLEDs with the same current density applied to the front two sections with the absorber operated O/C and S/C.
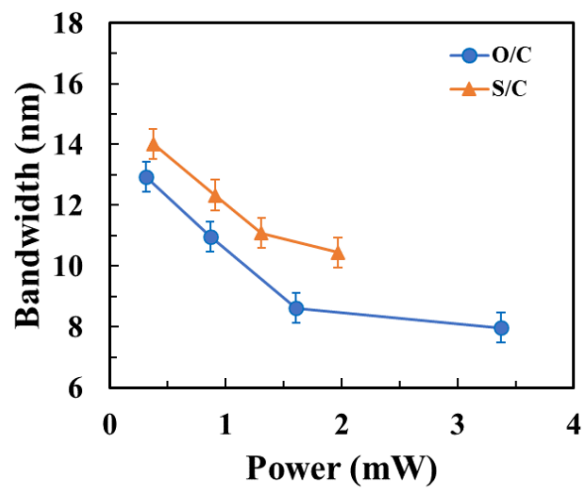
FIG. 4. Dependence of the optical properties on the three-section SLEDs with the same current density on the front two sections with the absorber operated O/C and S/C.
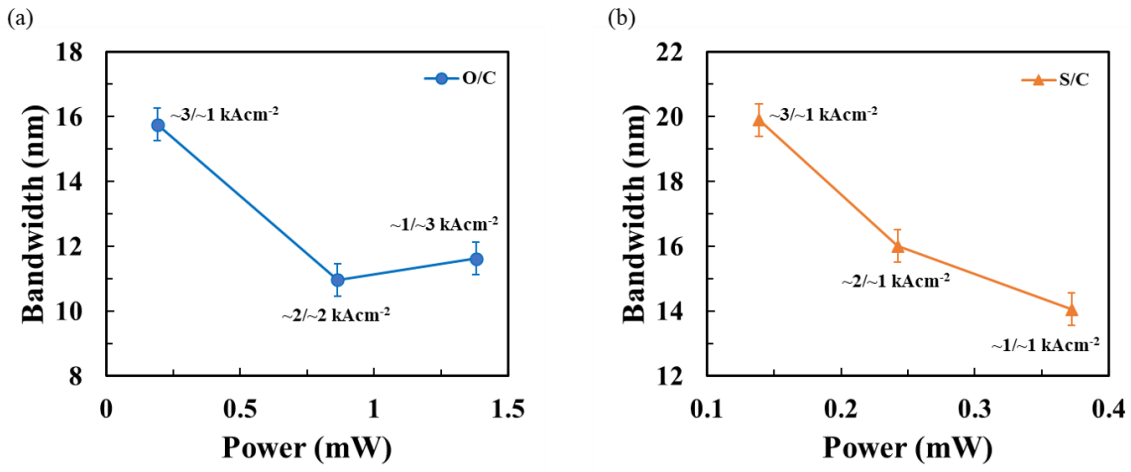
FIG. 5 Bandwidth as a function of output power for the three-section SLEDs with (a) O/C and (b) S/C absorber operation
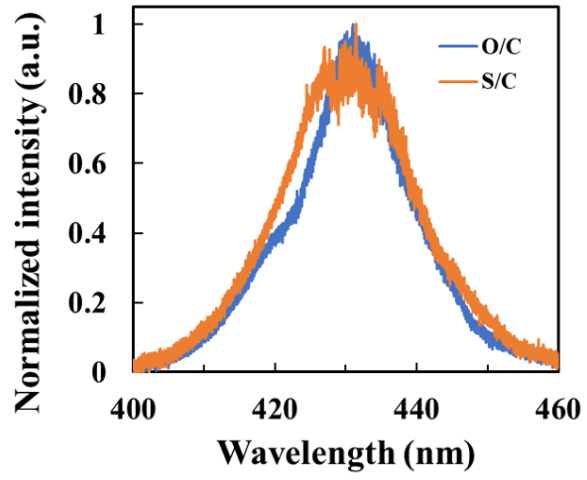
FIG. 6. The emission spectra of the three-section SLEDs under ~3/~1 kAcm^{-2} current injection in the gain sections with the absorber O/C and S/C.
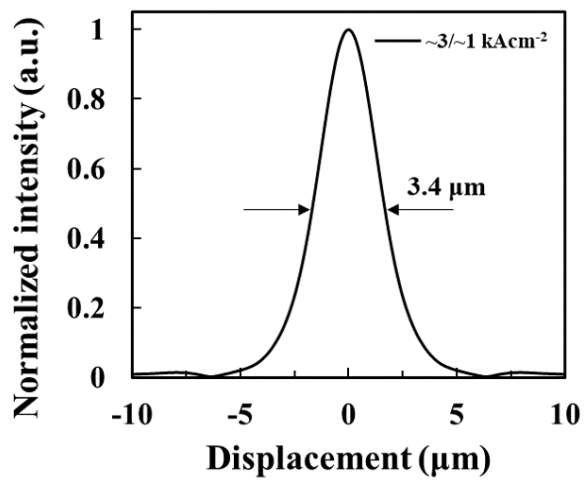
FIG. 7. IFT spectrum obtained from the ~3/~1 kAcm^{-2} three-section SLEDs with S/C absorber.